

# Hidden Cores of Active Galactic Nuclei as the Origin of Medium-Energy Neutrinos: Critical Tests with the MeV Gamma-Ray Connection

Kohta Murase,<sup>1, 2, 3, 4</sup> Shigeo S. Kimura,<sup>1, 2, 3</sup> and Peter Mészáros<sup>1, 2, 3</sup>

<sup>1</sup>Department of Physics, The Pennsylvania State University, University Park, Pennsylvania 16802, USA

<sup>2</sup>Department of Astronomy & Astrophysics, The Pennsylvania State University, University Park, Pennsylvania 16802, USA

<sup>3</sup>Center for Particle and Gravitational Astrophysics,

The Pennsylvania State University, University Park, Pennsylvania 16802, USA

<sup>4</sup>Yukawa Institute for Theoretical Physics, Kyoto, Kyoto 606-8502 Japan

The cores of active galactic nuclei (AGNs) are among the candidate sources of the IceCube neutrinos, but the underlying cosmic-ray acceleration processes are unclear. Based on the standard disk-corona picture of AGNs, we present a phenomenological model, in which protons are stochastically accelerated by turbulence from the magnetorotational instability. We show that this model can explain a large diffuse flux of about 30 TeV neutrinos if the cosmic rays carry a few percent of the coronal thermal energy. We find that the Bethe-Heitler process plays a crucial role in connecting these neutrinos and cascaded MeV gamma rays, and point out that the gamma-ray flux can be even enhanced by reacceleration of secondary pairs. Critical tests of the model are given by its prediction that a significant fraction of the MeV gamma-ray background correlates with the 10 TeV neutrino background, and nearby Seyfert galaxies should be seen by future MeV gamma-ray telescopes.

## I. INTRODUCTION

The origin of cosmic neutrinos observed in IceCube is a major enigma [1, 2], which has been deepened by the latest results on high- and medium-energy starting events and shower events [3–5]. The atmospheric background of high-energy electron neutrinos is much lower than that of muon neutrinos, allowing us to investigate the data below 100 TeV [6, 7]. The comparison with the extragalactic gamma-ray background (EGB) measured by *Fermi* indicates that the extragalactic neutrino background (ENB) at 10 – 100 TeV energies originates from hidden sources preventing the escape of GeV-TeV gamma rays [8].

Active galactic nuclei (AGNs) are major contributors to the energetics of high-energy cosmic radiations [9]; radio quiet (RQ) AGNs are dominant in the extragalactic x-ray sky [10–14], and radio loud (RL) AGNs including blazars give dominant contributions to the EGB [15–17]. AGNs may also explain the MeV gamma-ray background whose origin has been under debate (e.g., [18–20]).

High-energy neutrino production in the vicinity of supermassive black holes (SMBHs) were discussed early on [21–24], in particular to explain x-ray emission by cosmic-ray (CR) induced cascades assuming the existence of high Mach number accretion shocks at the inner edge of the disk [24–27]. However, cutoff features evident in the x-ray spectra of Seyfert galaxies and the absence of electron-positron annihilation lines ruled out the simple cascade scenario for the x-ray origin (e.g., [28, 29]). In the standard scenario, the observed x rays are attributed to thermal Comptonization of disk photons [30–34], and electrons are presumably heated in the coronal region [35, 36]. There has been significant progress in our understanding of accretion disks with the identification of the magnetorotational instability (MRI) [37, 38], which can result in the formation of a corona above the disk as a direct consequence of the accretion dynamics and magnetic dissipation (e.g., [39–45]).

Turbulence is also important for particle acceleration [46]. The roles of nonthermal particles have been studied in the context of radiatively inefficient accretion flows (RIAFs; [47, 48]), in which the plasma is often collisionless because Coulomb collisions are negligible for protons (e.g., [49–54]). Recent studies based on numerical simulations of the MRI [55, 56] support the idea that high-energy ions might be stochastically accelerated by the ensuing magnetohydrodynamic (MHD) turbulence.

The vicinity of SMBHs is often optically thick to GeV-TeV gamma rays, where CR acceleration cannot be directly probed by these photons, but high-energy neutrinos can be used as a unique probe of the physics of AGN cores. In this work, we present a concrete model for their high-energy emissions (see Fig. 1), in which spectral energy distributions (SEDs) are constructed from the data and from empirical relations. We compute neutrino and gamma-ray spectra, by solving both CR transport equations with the relevant energy losses and the resulting electromagnetic cascades of secondaries. We demonstrate the importance of future MeV gamma-ray observations for revealing the origin of IceCube neutrinos.

## II. PHENOMENOLOGICAL PRESCRIPTION OF AGN DISK CORONAE

We construct a phenomenological disk-corona model based on the existing data. SEDs of Seyfert galaxies have been extensively studied, which consist of several components; radio emission (see Ref. [57]), infrared emission from a dust torus [58], optical and ultraviolet components from an accretion disk [59], and x rays from a corona [31].

The averaged SEDs are provided in Ref. [60] as a function of the Eddington ratio,  $\lambda_{\text{Edd}} = L_{\text{bol}}/L_{\text{Edd}}$ , where  $L_{\text{bol}}$  and  $L_{\text{Edd}}$  are bolometric and Eddington luminosities, respectively. The well-known “blue” bump is attributed to multicolor blackbody emission from the geo-

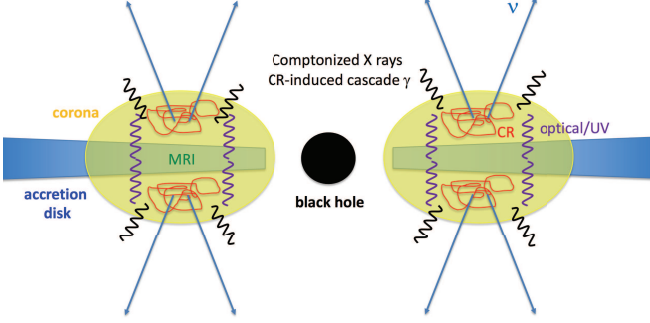


FIG. 1. Schematic picture of the AGN disk-corona scenario. Protons are accelerated by turbulence generated by the MRI in coronae, and produce high-energy neutrinos and cascaded gamma rays via interactions with matter and radiation.

metrically thin, optically thick disk [61]. The spectrum is expected to have an exponential cutoff at  $\varepsilon_{\text{disk,cut}} \approx 2.8k_B T_{\text{disk}}$ , where  $T_{\text{disk}} \approx 0.49(GM\dot{M}/16\pi\sigma_{\text{SB}}R_S^3)^{1/4}$  is the maximum effective temperature of the disk (e.g., [62]). Here,  $M$  is the SMBH mass,  $\dot{M}$  is the mass accretion rate, and  $R_S = 2GM/c^2$  is the Schwarzschild radius. Assuming a standard disk, we use  $\dot{M} \approx L_{\text{bol}}/(\eta_{\text{rad}}c^2)$  with a radiative efficiency of  $\eta_{\text{rad}} = 0.1$ . Although the spectra calculated by Ref. [60] extend to low energies, we only consider photons with  $\varepsilon_{\text{disk}} > 2$  eV because infrared photons would come from a dust torus.

X rays are produced via Compton upscattering by thermal electrons with  $T_e \sim 10^9$  K. The spectrum can be modeled by a power law with an exponential cutoff. The photon index,  $\Gamma_X$ , is correlated with the Eddington ratio as  $\Gamma_X \approx 0.167 \times \log(\lambda_{\text{Edd}}) + 2.0$  [63]. The cutoff energy is also given by  $\varepsilon_{X,\text{cut}} \sim [-74 \log(\lambda_{\text{Edd}}) + 1.5 \times 10^2]$  keV [29]. The electron temperature is written as  $k_B T_e \approx \varepsilon_{X,\text{cut}}/2$  for an optically thin corona. Then, assuming a slab geometry, the Thomson optical depth is given by  $\tau_T \approx 10^{(2.16-\Gamma_X)/1.06} (k_B T_e/\text{keV})^{-0.3}$  [29]. The x-ray luminosity  $L_X$  is converted into  $L_{\text{bol}}$  following Ref. [64], and the SMBH mass can be estimated by  $M \approx 2.0 \times 10^7 M_\odot (L_X/1.16 \times 10^{43} \text{ erg s}^{-1})^{0.746}$  [65]. The thus constructed SEDs are shown in Fig. 2.

We expect the disk coronae to be characterized by two temperatures, i.e.,  $T_p \gg T_e$  [66, 67] (see Appendix). We assume that the thermal protons are at the virial temperature,  $T_p \approx GMm_p/(3Rk_B)$ , where  $R = rR_S$  is the coronal size and  $r$  is the normalized radius. The normalized proton temperature is  $\theta_p = k_B T_p/(m_p c^2) \approx 5.3 \times 10^{-3} r_{1.5}^{-1}$ . With the sound speed  $C_s^2 \approx k_B T_p/m_p$  and Keplerian velocity  $V_K = \sqrt{GM/R}$ , the scale height is written as  $H \approx (C_s/V_K)R$ , leading to a nucleon target density,  $n_p \approx \tau_T/(\sigma_T H)$ . The magnetic field is estimated by  $B \approx \sqrt{8\pi m_p n_p k_B T_p/\beta}$ , where  $\beta$  is the plasma beta.

We summarize our model parameters in Table I. Note that most of the physical quantities can be estimated from the observational correlations. Thus, for a given

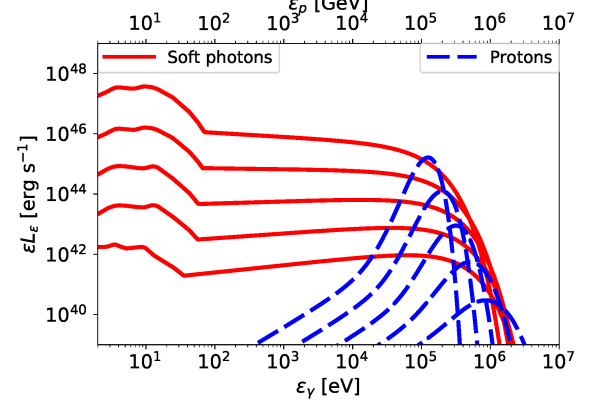


FIG. 2. Disk-corona SEDs and CR proton differential luminosities for  $L_X = 10^{42} \text{ erg s}^{-1}$ ,  $10^{43} \text{ erg s}^{-1}$ ,  $10^{44} \text{ erg s}^{-1}$ ,  $10^{45} \text{ erg s}^{-1}$ ,  $10^{46} \text{ erg s}^{-1}$ ,  $10^{47} \text{ erg s}^{-1}$  (from bottom to top).

TABLE I. Parameters used in this work. Units are  $[\text{erg s}^{-1}]$  for  $L_X$  and  $L_{\text{bol}}$ ,  $[M_\odot]$  for  $M$ ,  $[\text{cm}]$  for  $R$ ,  $[\text{cm}^{-3}]$  for  $n_p$ , and [%] for the ratio of the CR pressure to the thermal pressure.

$\log L_X$	$\log L_{\text{bol}}$	$\log M$	$\Gamma_X$	$\theta_e$	$\tau_T$	$\log R$	$\log n_p$	$P_{\text{CR}}/P_{\text{th}}$
42.0	43.0	6.51	1.72	0.27	0.59	13.5	10.73	0.27
43.0	44.2	7.25	1.80	0.23	0.52	14.2	9.93	0.54
44.0	45.4	8.00	1.88	0.20	0.46	15.0	9.13	0.94
45.0	46.6	8.75	1.96	0.16	0.41	15.7	8.33	1.54
46.0	47.9	9.49	2.06	0.12	0.36	16.4	7.53	2.34

$L_X$ ,  $\beta$  and  $r$  are the only remaining parameters. They are also constrained in a certain range by observations [68, 69] and numerical simulations [43, 45]. For example, recent MHD simulations show that  $\beta$  in the coronae can be as low as  $0.1 - 10$  (e.g., [39, 44]). We assume  $\beta \sim 1$ , and adopt  $r = 30$  throughout this work.

### III. STOCHASTIC ACCELERATION AND SECONDARY PRODUCTION IN CORONAE

For the disk coronae considered here, the infall and dissipation time scales are estimated to be  $t_{\text{fall}} \approx 2.5 \times 10^6 \text{ s } R_{15}(\alpha V_K/4000 \text{ km s}^{-1})^{-1}$  and  $t_{\text{diss}} \approx 1.8 \times 10^5 \text{ s } R_{15}(V_K/40000 \text{ km s}^{-1})^{-1} \beta^{1/2}$ , where  $\alpha$  is the viscosity parameter [61]. The electron relaxation time via Coulomb collisions,  $t_{ee,\text{rlx}} \sim 1.6 \times 10^3 \text{ s } \theta_{e,-0.6}^{3/2} \tau_T^{-1} R_{15}$ , is always shorter than  $t_{\text{diss}}$ . The proton relaxation time is much longer, which can ensure two temperature coronae (see Appendix). These collisionality arguments imply that turbulent acceleration is promising for not electrons but protons (although fast acceleration by small-scale reconnections might occur [70, 71]). The situation is somewhat analogous to that in RIAFs, for which nonthermal signatures have been studied (e.g., [72–74]).

We expect that protons are accelerated in the MHD

turbulence. We compute steady state CR spectra by solving the following Fokker-Planck equation (e.g., [75–78]),

$$\frac{\partial F_p}{\partial t} = \frac{1}{\varepsilon_p^2} \frac{\partial}{\partial \varepsilon_p} \left( \varepsilon_p^2 D_{\varepsilon_p} \frac{\partial F_p}{\partial \varepsilon_p} + \frac{\varepsilon_p^3}{t_{p-\text{cool}}} F_p \right) - \frac{F_p}{t_{\text{esc}}} + \dot{F}_{p,\text{inj}}, \quad (1)$$

where  $F_p$  is the CR distribution function,  $D_{\varepsilon_p} \approx \varepsilon_p^2/t_{\text{acc}}$  is the diffusion coefficient in energy space,  $t_{p-\text{cool}}^{-1} = t_{pp}^{-1} + t_{p\gamma}^{-1} + t_{\text{BH}}^{-1} + t_{p-\text{syn}}^{-1}$  is the total cooling rate,  $t_{\text{esc}}^{-1} = t_{\text{fall}}^{-1} + t_{\text{diff}}$  is the escape rate, and  $\dot{F}_{p,\text{inj}}$  is the injection function (see Appendix [79]). The stochastic acceleration time is given by  $t_{\text{acc}} \approx \eta(c/V_A)^2 (R/c) (\varepsilon_p/eBR)^{2-q}$ , where  $V_A$  is the Alfvén velocity and  $\eta$  is the inverse of the turbulence strength [80, 81]. We adopt  $q = 5/3$ , which is consistent with the recent MHD simulations [56], together with  $\eta = 10$ . Because the dissipation rate in the coronae is expected to be proportional to  $L_X$ , we assume that the injection function linearly scales as  $L_X$ . To explain the ENB, the CR pressure required for  $L_X = 10^{44} \text{ erg s}^{-1}$  turns out to be  $\sim 1\%$  of the thermal pressure, which is reasonable. We plot  $\varepsilon_p L_{\varepsilon_p} \equiv 4\pi (\varepsilon_p^4/c^3) F_p \mathcal{V} (t_{\text{esc}}^{-1} + t_{p-\text{cool}}^{-1})$  in Fig. 2, where  $\mathcal{V}$  is the volume.

While the CRs are accelerated, they interact with matter and radiation modeled in the previous section, and produce secondary particles. Following Ref. [82, 83], we solve the kinetic equations taking into account electromagnetic cascades. In this work, secondary injections by the Bethe-Heitler and  $p\gamma$  processes are approximately treated as  $\varepsilon_e^2 (dN_e^{\text{BH}}/d\varepsilon_e)|_{\varepsilon_e=(m_e/m_p)\varepsilon_p} \approx t_{\text{BH}}^{-1} \varepsilon_p^2 (dN_{\text{CR}}/d\varepsilon_p)$ ,  $\varepsilon_e^2 (dN_e^{p\gamma}/d\varepsilon_e)|_{\varepsilon_e=0.05\varepsilon_p} \approx (1/3) \varepsilon_{\nu}^2 (dN_{\nu}^{p\gamma}/d\varepsilon_{\nu})|_{\varepsilon_{\nu}=0.05\varepsilon_p} \approx (1/8) t_{p\gamma}^{-1} \varepsilon_p^2 (dN_{\text{CR}}/d\varepsilon_p)$ , and  $\varepsilon_{\gamma}^2 (dN_{\gamma}^{p\gamma}/d\varepsilon_{\gamma})|_{\varepsilon_{\gamma}=0.1\varepsilon_p} \approx (1/2) t_{p\gamma}^{-1} \varepsilon_p^2 (dN_{\text{CR}}/d\varepsilon_p)$ . The resulting cascade spectra are broad, being determined by synchrotron and inverse Compton emission.

In general, stochastic acceleration models naturally predict reacceleration of secondary pairs populated by cascades [84]. The critical energy of the pairs,  $\varepsilon_{e,\text{cl}}$ , is consistently determined by the balance between the acceleration time  $t_{\text{acc}}$  and the electron cooling time  $t_{e-\text{cool}}$ . We find that whether the secondary reacceleration occurs or not is rather sensitive to  $B$  and  $t_{\text{acc}}$ . For example, with  $\beta = 3$  and  $q = 1.5$ , the reaccelerated pairs can upscatter x-ray photons up to  $\sim (\varepsilon_{e,\text{cl}}/m_e c^2)^2 \varepsilon_X \simeq 3.4 \text{ MeV} (\varepsilon_{e,\text{cl}}/30 \text{ MeV})^2 (\varepsilon_X/1 \text{ keV})$ , which may form a gamma-ray tail. However, if  $\varepsilon_{e,\text{cl}} \lesssim 1 \text{ MeV}$  (for  $\beta = 1$  and  $q = 5/3$ ), reacceleration is negligible, and small-scale turbulence is more likely to be dissipated at high  $T_p$  [85].

#### IV. NEUTRINO BACKGROUND AND MEV GAMMA-RAY CONNECTION

We calculate neutrino and gamma-ray spectra for different source luminosities, and obtain the EGB and ENB through Eq. (31) of Ref. [91]. We use the x-ray luminosity function  $d\rho_X/dL_X$ , given by Ref. [14], taking into account a factor of 2 enhancement by Compton thick

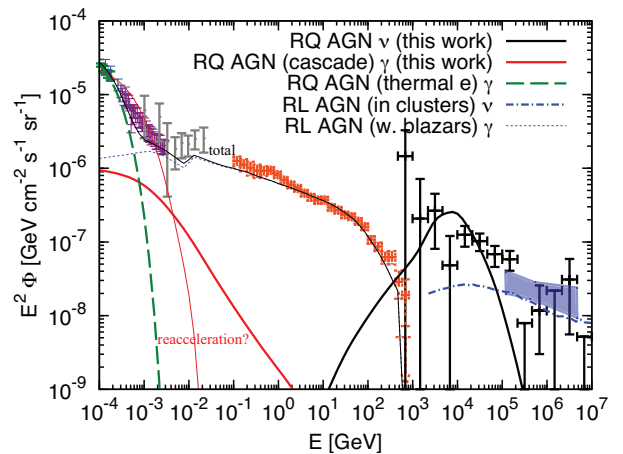


FIG. 3. EGB and ENB spectra in our RQ AGN core model. The data are taken from *Swift-BAT* [86] (green), Nagoya balloon [87] (blue), SMM [88] (purple), COMPTEL [89] (gray), *Fermi-LAT* [90] (orange), and IceCube [5] for shower (black) and upgoing muon track (blue shaded) events. A possible contribution of reaccelerated pairs is indicated (thin solid).

AGNs. Results are shown in Fig. 3. Our RQ AGN core model can explain the ENB at  $\sim 30 \text{ TeV}$  energies if the CR pressure is  $\sim 1\%$  of the thermal pressure.

In the vicinity of SMBHs, high-energy neutrinos are produced by *both*  $pp$  and  $p\gamma$  interactions. The disk-corona model indicates  $\tau_T \sim 1$  (see Table 1), which leads to the effective  $pp$  optical depth  $f_{pp} \approx t_{\text{esc}}/t_{pp} \approx n_p (\kappa_{pp} \sigma_{pp}) R (c/V_{\text{fall}}) \sim 2\tau_T (\alpha V_K/4000 \text{ km s}^{-1})^{-1}$ . Note that  $V_K$  is a function of  $M$  (and  $L_X$ ). X-ray photons from coronae provide target photons for the photomeson production, whose effective optical depth [8, 92] is  $f_{p\gamma}[\varepsilon_p] \approx t_{\text{esc}}/t_{p\gamma} \approx \eta_{p\gamma} \hat{\sigma}_{p\gamma} R (c/V_{\text{fall}}) n_X (\varepsilon_p/\tilde{\varepsilon}_{p\gamma-X})^{\Gamma_X-1} \sim 0.9 L_{X,44} R_{15}^{-1} (\alpha V_K/4000 \text{ km s}^{-1})^{-1} (1 \text{ keV}/\varepsilon_X) \eta_{p\gamma} (\varepsilon_p/\tilde{\varepsilon}_{p\gamma-X})^{\Gamma_X-1}$ , where  $\eta_{p\gamma} \approx 2/(1 + \Gamma_X)$ ,  $\hat{\sigma}_{p\gamma} \sim 0.7 \times 10^{-28} \text{ cm}^2$  is the attenuation cross section,  $\tilde{\varepsilon}_{\Delta} \sim 0.3 \text{ GeV}$ ,  $\tilde{\varepsilon}_{p\gamma-X} = 0.5 m_p c^2 \tilde{\varepsilon}_{\Delta} / \varepsilon_X \simeq 0.14 \text{ PeV} (\varepsilon_X/1 \text{ keV})^{-1}$ , and  $n_X \sim L_X/(4\pi R^2 c \varepsilon_X)$  is used. The total meson production optical depth is given by  $f_{\text{mes}} = f_{p\gamma} + f_{pp}$ , which always exceeds unity in our model.

Importantly,  $\sim 10 - 100 \text{ TeV}$  neutrinos originate from CRs with  $\sim 0.2 - 2 \text{ PeV}$ . Different from previous studies explaining the IceCube data [93, 94], disk photons are irrelevant for the photomeson production because its threshold energy is  $\tilde{\varepsilon}_{p\gamma-\text{th}} \simeq 3.4 \text{ PeV} (\varepsilon_{\text{disk}}/10 \text{ eV})^{-1}$ . However, CRs in the 0.1-1 PeV range should efficiently interact with disk photons via the Bethe-Heitler process because the characteristic energy is  $\tilde{\varepsilon}_{\text{BH-disk}} = 0.5 m_p c^2 \tilde{\varepsilon}_{\text{BH}} / \varepsilon_{\text{disk}} \simeq 0.47 \text{ PeV} (\varepsilon_{\text{disk}}/10 \text{ eV})^{-1}$ , where  $\tilde{\varepsilon}_{\text{BH}} \sim 10(2m_e c^2) \sim 10 \text{ MeV}$  [95, 96]. Approximating the number of disk photons by  $n_{\text{disk}} \sim L_{\text{bol}}/(4\pi R^2 c \varepsilon_{\text{disk}})$ , the Bethe-Heitler effective optical depth [97] is estimated to be  $f_{\text{BH}} \approx n_{\text{disk}} \hat{\sigma}_{\text{BH}} R (c/V_{\text{fall}}) \sim 20 L_{\text{bol},45.3} R_{15}^{-1} (\alpha V_K/4000 \text{ km s}^{-1})^{-1} (10 \text{ eV}/\varepsilon_{\text{disk}})$ ,

where  $\hat{\sigma}_{\text{BH}} \sim 0.8 \times 10^{-30} \text{ cm}^2$ . The dominance of the Bethe-Heitler process is a direct consequence of the observed disk-corona SEDs, implying that the medium-energy neutrino flux is suppressed by  $\sim f_{\text{mes}}/f_{\text{BH}}$ .

The ENB flux is analytically estimated to be

$$E_\nu^2 \Phi_\nu \sim 10^{-7} \text{ GeV cm}^{-2} \text{ s}^{-1} \text{ sr}^{-1} \left( \frac{2K}{1+K} \right) \xi_{\text{CR}} \mathcal{R}_{p,0.5}^{-1} \times \left( \frac{20f_{\text{mes}}}{1+f_{\text{BH}}+f_{\text{mes}}} \right) L_{X,44} \left( \frac{\xi_z \rho_X}{10^{-5} \text{ Mpc}^{-3}} \right). \quad (2)$$

where  $K = 1$  and  $K = 2$  for  $p\gamma$  and  $pp$  interactions, respectively, and  $\xi_z \sim 3$  represents the redshift evolution of RQ AGNs. Eq. (2) is consistent with the numerical results presented in Fig. 3. Here  $\mathcal{R}_p$  is the conversion factor from bolometric to differential luminosities,  $\xi_{\text{CR}}$  is the CR loading parameter defined against the x-ray luminosity, and  $P_{\text{CR}}/P_{\text{th}} \sim 0.01$  corresponds to  $\xi_{\text{CR}} \sim 1$  in our model. We find that the ENB and EGB are dominated by AGNs with  $L_X \sim 10^{44} \text{ erg s}^{-1}$ , at which the local number density is  $\rho_X \sim 3 \times 10^{-6} \text{ Mpc}^{-3}$  [98].

The  $pp$ ,  $p\gamma$  and Bethe-Heitler processes all initiate electromagnetic cascades, whose emission appears in the MeV range. Thanks to the dominance of the Bethe-Heitler process, RQ AGNs responsible for the medium-energy ENB should contribute to  $\gtrsim 10 - 30\%$  of the MeV EGB. Possible reacceleration can enhance the MeV gamma-ray flux, and the MeV EGB could be explained if  $\sim 0.1\%$  of the pairs is injected into the reacceleration process. For comparison, models for RL AGNs ([99, 100] for the EGB and [101] for the ENB) are also shown in Fig. 3. This demonstrates that in principle the dominant portions of the EGB and ENB from MeV to PeV energies can be explained by the combination of RQ AGNs and RL AGNs. However, we also caution that other possibilities such as starburst galaxies are still viable [102].

## V. MULTIMESSENGER TESTS

Detecting MeV signals from individual Seyferts would be crucial for testing the model, which is challenging for existing gamma-ray telescopes. However, this would be feasible with future telescopes like eASTROGAM [103], GRAMS [107], and AMEGO [104] (see Fig. 4).

For luminous Seyfert galaxies, the fact that x rays come from thermal Comptonization suggests that the photon energy density is larger than the magnetic field energy density. In the scenario to explain 10-100 TeV neutrinos, secondary pairs are injected in the 100-300 GeV range and form a fast cooling  $\varepsilon_e^{-2}$  spectrum down to MeV energies in the steady state. Thus, in the simple inverse Compton cascade scenario, the cascade spectrum is extended up to the break energy due to  $\gamma\gamma \rightarrow e^+e^-$ . In reality, both synchrotron and inverse Compton processes can be important. The characteristic frequency of synchrotron emission by Bethe-Heitler pairs is given by  $\varepsilon_{\text{syn}}^{\text{BH}} \sim 0.8 \text{ MeV } B_{2.5}(\varepsilon_p/0.5 \text{ PeV})^2$  [83]. Because

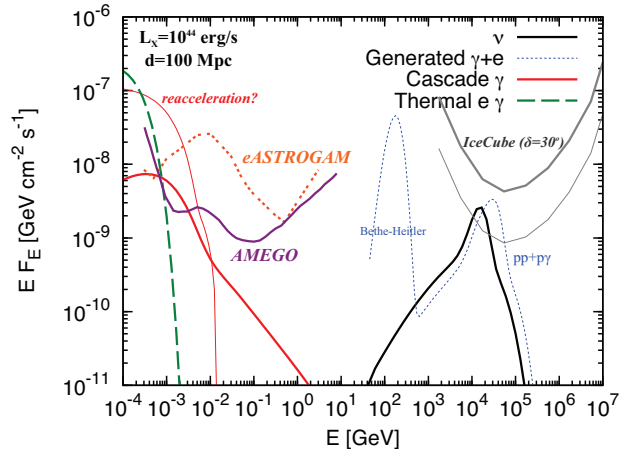


FIG. 4. Point source fluxes of all flavor neutrinos and gamma rays from a nearby RQ AGN. A possible effect of secondary reacceleration is indicated (thin solid). For eASTROGAM [103] and AMEGO [104] sensitivities, the observation time of  $10^6$  s is assumed. The IceCube eight-year sensitivity [105] and the 5 times better case [106] are shown.

disk photons lie in the  $\sim 1 - 10$  eV range, the Klein-Nishina effect is moderately important at the injection energies. The synchrotron cascade is dominant if the photon energy density is smaller than  $\sim 10B^2/(8\pi)$ , i.e.,  $B \gtrsim 200 \text{ G } L_{\text{bol},45.3}^{1/2} R_{15}^{-1}$ . In either synchrotron or inverse Compton cascades, MeV gamma rays are expected.

The ENB and EGB are dominated by AGNs with  $L_X \sim 10^{44} \text{ erg s}^{-1}$ . AMEGO's differential sensitivity suggests that point sources with  $d \lesssim 150 - 400 \text{ Mpc}$  are detectable, and the number of the sources within this horizon is  $\mathcal{N}_{\text{AGN}} \sim 10 - 100$ . Detections or nondetections of the MeV gamma-ray counterparts will support or falsify the AGN core model as the origin of  $\sim 30$  TeV neutrinos. Note that the predicted neutrino flux shown in Fig. 4 is below the current IceCube sensitivity. Nearby Seyferts may be seen as point sources with IceCube-Gen2, but stacking analyses are more promising.

## VI. SUMMARY AND DISCUSSION

We presented the results of a concrete model for RQ AGNs which can explain the medium-energy neutrino data. The disk-corona SEDs have been well studied, and known empirical relations enabled us to estimate model parameters, with which we solved the relevant transport equations and computed subsequent cascades consistently. The model is not only motivated from both observations and theories but it also provides clear predictions. In particular, the dominance of the Bethe-Heitler process is a direct consequence of the observed SEDs, leading to a robust MeV gamma-ray connection. Nearby Seyferts will be promising targets for future MeV gamma-ray telescopes such as eASTROGAM and AMEGO. A

good fraction of the MeV EGB may come from RQ AGNs especially in the presence of secondary reacceleration, in which gamma-ray anisotropy searches should be powerful tools [108]. Neutrino multiplet and stacking searches with IceCube-Gen2 are also promising [98].

The suggested tests are crucial for unveiling nonthermal phenomena in the vicinity of SMBHs. For low-luminosity AGNs, where the plasma density is low, direct acceleration may occur [109] and TeV gamma rays can escape [110]. However, in Seyferts, the plasma density is so high that a gap is not expected, and GeV-TeV gamma rays are blocked. Only MeV gamma rays can escape from the core region, and neutrinos serve as a smoking gun.

Our results strengthen the importance of further theoretical studies of disk-corona systems. Simulations on turbulent acceleration in coronae and particle-in-cell computations of acceleration via magnetic reconnections are encouraged in order to understand the CR acceleration in the disk-corona system. Global MHD simulations will also be relevant to examine other postulates such as accretion shocks [24, 25, 111, 112] or colliding blobs [113] and to reveal the origin of low-frequency emission that could come from the outer region of coronae [114, 115].

## ACKNOWLEDGMENTS

This work is supported by Alfred P. Sloan Foundation and NSF Grant No. PHY-1620777 (K.M.), JSPS Oversea Research Fellowship and the IGC post-doctoral fellowship program (S.S.K.), and NASA NNX13AH50G as well as the Eberly Foundation (P.M.). While we were finalizing this project, we became aware of a related work by Inoue et al. (arXiv:1904.00554). We thank for Yoshiyuki Inoue for discussions. Both works are independent and complementary, and there are notable differences. We consider stochastic acceleration by turbulence based on the disk-corona model rather than by accretion shocks. Also, we focus on the origin of 10-100 TeV neutrinos, for which the Bethe-Heitler suppression is critical. Third, we calculate CR-induced electromagnetic cascades, which is critical for testing the scenario for IceCube neutrinos. K.M. also thanks for the invitation to the AMEGO Splitter meeting held in January 2019, in which preliminary results of cascade emission were presented.

---

[1] M. Aartsen *et al.* (IceCube Collaboration), Phys.Rev.Lett. **111**, 021103 (2013), arXiv:1304.5356 [astro-ph.HE].

[2] M. Aartsen *et al.* (IceCube Collaboration), Science **342**, 1242856 (2013), arXiv:1311.5238 [astro-ph.HE].

[3] M. Aartsen *et al.* (IceCube Collaboration), Phys.Rev. **D91**, 022001 (2015), arXiv:1410.1749 [astro-ph.HE].

[4] M. G. Aartsen *et al.* (IceCube Collaboration), Astrophys. J. **809**, 98 (2015), arXiv:1507.03991 [astro-ph.HE].

[5] M. G. Aartsen *et al.* (IceCube Collaboration), (2017), arXiv:1710.01191 [astro-ph.HE].

[6] J. F. Beacom and J. Candia, JCAP **0411**, 009 (2004), arXiv:hep-ph/0409046 [hep-ph].

[7] R. Laha, J. F. Beacom, B. Dasgupta, S. Horuchi, and K. Murase, Phys.Rev. **D88**, 043009 (2013), arXiv:1306.2309 [astro-ph.HE].

[8] K. Murase, D. Guetta, and M. Ahlers, Phys. Rev. Lett. **116**, 071101 (2016), arXiv:1509.00805 [astro-ph.HE].

[9] K. Murase and M. Fukugita, Phys. Rev. **D99**, 063012 (2019), arXiv:1806.04194 [astro-ph.HE].

[10] A. C. Fabian and X. Barcons, Annual Review of Astronomy and Astrophysics **30**, 429 (1992).

[11] Y. Ueda, M. Akiyama, K. Ohta, and T. Miyaji, ApJ **598**, 886 (2003), astro-ph/0308140.

[12] G. Hasinger, T. Miyaji, and M. Schmidt, Astron. Astrophys. **441**, 417 (2005), arXiv:astro-ph/0506118 [astro-ph].

[13] M. Ajello *et al.*, Astrophys. J. **689**, 666 (2008), arXiv:0808.3377 [astro-ph].

[14] Y. Ueda, M. Akiyama, G. Hasinger, T. Miyaji, and M. G. Watson, Astrophys.J. **786**, 104 (2014), arXiv:1402.1836 [astro-ph.CO].

[15] L. Costamante, Int.J.Mod.Phys. **D22**, 1330025 (2013), arXiv:1309.0612 [astro-ph.HE].

[16] Y. Inoue, in *5th International Fermi Symposium Nagoya, Japan, October 20-24, 2014* (2014) arXiv:1412.3886 [astro-ph.HE].

[17] M. Fornasa and M. A. Sanchez-Conde, Phys. Rept. **598**, 1 (2015), arXiv:1502.02866 [astro-ph.CO].

[18] Y. Inoue, T. Totani, and Y. Ueda, Astrophys. J. **672**, L5 (2008), arXiv:0709.3877 [astro-ph].

[19] M. Ajello *et al.*, Astrophys. J. **699**, 603 (2009), arXiv:0905.0472 [astro-ph.CO].

[20] A. Lien and B. D. Fields, Astrophys. J. **747**, 120 (2012), arXiv:1201.3447 [astro-ph.CO].

[21] D. Eichler, Astrophys. J. **232**, 106 (1979).

[22] V. S. Berezinskii and V. L. Ginzburg, MNRAS **194**, 3 (1981).

[23] M. C. Begelman, B. Rudak, and M. Sikora, ApJ **362**, 38 (1990).

[24] F. W. Stecker, C. Done, M. H. Salamon, and P. Sommers, Phys.Rev.Lett. **66**, 2697 (1991).

[25] D. Kazanas and D. C. Ellison, ApJ **304**, 178 (1986).

[26] A. A. Zdziarski, ApJ **305**, 45 (1986).

[27] M. Sikora, J. G. Kirk, M. C. Begelman, and P. Schneider, ApJ **320**, L81 (1987).

[28] T. Di Matteo, (1999), arXiv:astro-ph/9912221 [astro-ph].

[29] C. Ricci, L. C. Ho, A. C. Fabian, B. Trakhtenbrot, M. J. Koss, Y. Ueda, A. Lohfink, T. Shimizu, F. E. Bauer, R. Mushotzky, K. Schawinski, S. Paltani, I. Lamperti,

E. Treister, and K. Oh, MNRAS **480**, 1819 (2018), arXiv:1809.04076 [astro-ph.HE].

[30] S. L. Shapiro, A. P. Lightman, and D. M. Eardley, *Astrophys. J.* **204**, 187 (1976).

[31] R. A. Sunyaev and L. G. Titarchuk, *A&A* **500**, 167 (1980).

[32] A. A. Zdziarski, W. N. Johnson, and P. Magdziarz, *Mon. Not. Roy. Astron. Soc.* **283**, 193 (1996), arXiv:astro-ph/9607015 [astro-ph].

[33] J. Poutanen and R. Svensson, *ApJ* **470**, 249 (1996), arXiv:astro-ph/9605073 [astro-ph].

[34] F. Haardt, L. Maraschi, and G. Ghisellini, *Astrophys. J.* **476**, 620 (1997), arXiv:astro-ph/9609050 [astro-ph].

[35] E. P. T. Liang and R. H. Price, *ApJ* **218**, 247 (1977).

[36] A. A. Galeev, R. Rosner, and G. S. Vaiana, *Astrophys. J.* **229**, 318 (1979).

[37] S. A. Balbus and J. F. Hawley, *ApJ* **376**, 214 (1991).

[38] S. A. Balbus and J. F. Hawley, *Reviews of Modern Physics* **70**, 1 (1998).

[39] K. A. Miller and J. M. Stone, *Astrophys. J.* **534**, 398 (2000), arXiv:astro-ph/9912135 [astro-ph].

[40] A. Merloni and A. C. Fabian, *Mon. Not. Roy. Astron. Soc.* **321**, 549 (2001), arXiv:astro-ph/0009498 [astro-ph].

[41] B. F. Liu, S. Mineshige, F. Meyer, E. Meyer-Hofmeister, and T. Kawaguchi, *Astrophys. J.* **575**, 117 (2002), arXiv:astro-ph/0204174 [astro-ph].

[42] E. G. Blackman and M. E. Pesah, *Astrophys. J.* **704**, L113 (2009), arXiv:0907.2068 [astro-ph.HE].

[43] Y. Io and T. K. Suzuki, *Astrophys. J.* **780**, 46 (2014), arXiv:1308.6427 [astro-ph.SR].

[44] T. K. Suzuki and S.-i. Inutsuka, *ApJ* **784**, 121 (2014), arXiv:1309.6916 [astro-ph.EP].

[45] Y.-F. Jiang, J. M. Stone, and S. W. Davis, *Astrophys. J.* **784**, 169 (2014), arXiv:1402.2979 [astro-ph.HE].

[46] A. Lazarian, L. Vlahos, G. Kowal, H. Yan, A. Beresnyak, and E. M. de Gouveia Dal Pino, *Space Sci. Rev.* **173**, 557 (2012), arXiv:1211.0008 [astro-ph.SR].

[47] R. Narayan and I. Yi, *ApJ* **428**, L13 (1994), astro-ph/9403052.

[48] F. Yuan and R. Narayan, *ARA&A* **52**, 529 (2014), arXiv:1401.0586 [astro-ph.HE].

[49] F. Takahara and M. Kusunose, *Progress of Theoretical Physics* **73**, 1390 (1985).

[50] R. Mahadevan, R. Narayan, and J. Krolik, *Astrophys. J.* **486**, 268 (1997), arXiv:astro-ph/9704018 [astro-ph].

[51] R. Mahadevan and E. Quataert, *Astrophys. J.* **490**, 605 (1997), arXiv:astro-ph/9705067 [astro-ph].

[52] S. S. Kimura, K. Toma, and F. Takahara, *ApJ* **791**, 100 (2014), arXiv:1407.0115 [astro-ph.HE].

[53] J. W. Lynn, E. Quataert, B. D. G. Chandran, and I. J. J. Parrish, *ApJ* **791**, 71 (2014), arXiv:1403.3123 [astro-ph.HE].

[54] D. Ball, F. Ozel, D. Psaltis, C.-K. Chan, and L. Sironi, *Astrophys. J.* **853**, 184 (2018), arXiv:1705.06293 [astro-ph.HE].

[55] S. S. Kimura, K. Toma, T. K. Suzuki, and S.-i. Inutsuka, *Astrophys. J.* **822**, 88 (2016), arXiv:1602.07773 [astro-ph.HE].

[56] S. S. Kimura, K. Tomida, and K. Murase, *Mon. Not. Roy. Astron. Soc.* **485**, 163 (2019), arXiv:1812.03901 [astro-ph.HE].

[57] F. Panessa, R. D. Baldi, A. Laor, P. Padovani, E. Behar, and I. McHardy, arXiv e-prints , arXiv:1902.05917 (2019), arXiv:1902.05917 [astro-ph.GA].

[58] H. Netzer, *Ann. Rev. Astron. Astrophys.* **53**, 365 (2015), arXiv:1505.00811 [astro-ph.GA].

[59] A. Koratkar and O. Blaes, *Publ. Astron. Soc. Pac.* **111**, 1 (1999).

[60] L. C. Ho, *ARA&A* **46**, 475 (2008), arXiv:0803.2268.

[61] N. I. Shakura and R. A. Sunyaev, *Astron. Astrophys.* **24**, 337 (1973).

[62] J. E. Pringle, *ARA&A* **19**, 137 (1981).

[63] B. Trakhtenbrot, C. Ricci, M. J. Koss, K. Schawinski, R. Mushotzky, Y. Ueda, S. Veilleux, I. Lamperti, K. Oh, E. Treister, D. Stern, F. Harrison, M. Baloković, and N. Gehrels, *MNRAS* **470**, 800 (2017), arXiv:1705.01550 [astro-ph.GA].

[64] P. F. Hopkins, G. T. Richards, and L. Hernquist, *ApJ* **654**, 731 (2007), arXiv:astro-ph/0605678 [astro-ph].

[65] J. A. Mayers, K. Romer, A. Fahari, J. P. Stott, P. Giles, P. J. Rooney, A. Bermeo-Hernandez, C. A. Collins, M. Hilton, B. Hoyle, A. R. Liddle, R. G. Mann, C. J. Miller, R. C. Nichol, M. Sahlén, C. Vergara-Cervantes, and P. T. P. Viana, arXiv e-prints , arXiv:1803.06891 (2018), arXiv:1803.06891 [astro-ph.GA].

[66] T. Di Matteo, E. G. Blackman, and A. C. Fabian, *Mon. Not. Roy. Astron. Soc.* **291**, L23 (1997), arXiv:astro-ph/9705079 [astro-ph].

[67] X. Cao, *Mon. Not. Roy. Astron. Soc.* **394**, 207 (2009), arXiv:0812.1828 [astro-ph].

[68] C. Jin, M. Ward, C. Done, and J. Gelbord, *MNRAS* **420**, 1825 (2012), arXiv:1109.2069 [astro-ph.HE].

[69] C. W. Morgan *et al.*, *Astrophys. J.* **756**, 52 (2012), arXiv:1205.4727 [astro-ph.CO].

[70] M. Hoshino, *Phys. Rev. Lett.* **114**, 061101 (2015), arXiv:1502.02452 [astro-ph.HE].

[71] X. Li, F. Guo, H. Li, and G. Li, *Astrophys. J.* **811**, L24 (2015), arXiv:1505.02166 [astro-ph.SR].

[72] F. Ozel, D. Psaltis, and R. Narayan, *Astrophys. J.* **541**, 234 (2000), arXiv:astro-ph/0004195 [astro-ph].

[73] S. S. Kimura, K. Murase, and K. Toma, *Astrophys. J.* **806**, 159 (2015), arXiv:1411.3588 [astro-ph.HE].

[74] D. Ball, F. Ozel, D. Psaltis, and C.-k. Chan, *Astrophys. J.* **826**, 77 (2016), arXiv:1602.05968 [astro-ph.HE].

[75] P. A. Becker, T. Le, and C. D. Dermer, *Astrophys. J.* **647**, 539 (2006), arXiv:astro-ph/0604504 [astro-ph].

[76] L. Stawarz and V. Petrosian, *Astrophys. J.* **681**, 1725 (2008), arXiv:0803.0989 [astro-ph].

[77] J. S. Chang and G. Cooper, *Journal of Computational Physics* **6**, 1 (1970).

[78] B. T. Park and V. Petrosian, The Astrophysical Journal Supplement Series **103**, 255 (1996).

[79] We consider meson production processes by  $pp$  ( $t_{pp}$ ) and  $p\gamma$  ( $t_{p\gamma}$ ) interactions, as well as the Bethe-Heitler pair production ( $t_{BH}$ ), proton synchrotron radiation ( $t_{p-syn}$ ), diffusive escape ( $t_{diff}$ ), and infall losses ( $t_{fall}$ ).

[80] C. D. Dermer, J. A. Miller, and H. Li, *Astrophys. J.* **456**, 106 (1996), arXiv:astro-ph/9508069 [astro-ph].

[81] C. D. Dermer, K. Murase, and Y. Inoue, *JHEAp* **3-4**, 29 (2014), arXiv:1406.2633 [astro-ph.HE].

[82] K. Murase, *Phys. Rev.* **D97**, 081301(R) (2018), arXiv:1705.04750 [astro-ph.HE].

[83] K. Murase, A. Franckowiak, K. Maeda, R. Margutti, and J. F. Beacom, *Astrophys. J.* **874**, 80 (2019), arXiv:1807.01460 [astro-ph.HE].

[84] K. Murase, K. Asano, T. Terasawa, and P. Meszaros, *Astrophys. J.* **746**, 164 (2012), arXiv:1107.5575 [astro-ph.HE].

[85] G. G. Howes, J. M. Tenbarge, W. Dorland, E. Quataert, A. A. Schekochihin, R. Numata, and T. Tatsumi, *Phys. Rev. Lett.* **107**, 035004 (2011), arXiv:1104.0877 [astro-ph.SR].

[86] M. Ajello, R. W. Romani, D. Gasparrini, M. S. Shaw, J. Bolmer, G. Cotter, J. Finke, J. Greiner, S. E. Healey, O. King, W. Max-Moerbeck, P. F. Michelson, W. J. Potter, A. Rau, A. C. S. Readhead, J. L. Richards, and P. Schady, *ApJ* **780**, 73 (2014), arXiv:1310.0006 [astro-ph.CO].

[87] Y. Fukuda, S. Hayakawa, I. Kasahara, F. Makino, Y. Tanaka, and B. V. Sreekantan, *Nature* **254**, 398 (1975).

[88] K. Watanabe, D. H. Hartmann, M. D. Leising, L. S. The, G. H. Share, and R. L. Kinzer, in *Proceedings of the Fourth Compton Symposium*, American Institute of Physics Conference Series, Vol. 410, edited by C. D. Dermer, M. S. Strickman, and J. D. Kurfess (1997) pp. 1223–1227.

[89] G. Weidenspointner, M. Varendorff, S. C. Kappadath, K. Bennett, H. Bloemen, R. Diehl, W. Hermse, G. G. Lichti, J. Ryan, and V. Schönfelder, in *American Institute of Physics Conference Series*, Vol. 510, edited by M. L. McConnell and J. M. Ryan (2000) pp. 467–470.

[90] M. Ackermann *et al.* (Fermi LAT collaboration), *Astrophys. J.* **799**, 86 (2015), arXiv:1410.3696 [astro-ph.HE].

[91] K. Murase, Y. Inoue, and C. D. Dermer, *Phys. Rev. D* **90**, 023007 (2014), arXiv:1403.4089 [astro-ph.HE].

[92] K. Murase, K. Ioka, S. Nagataki, and T. Nakamura, *Phys. Rev. D* **78**, 023005 (2008), arXiv:0801.2861 [astro-ph].

[93] F. W. Stecker, *Phys. Rev. D* **88**, 047301 (2013), arXiv:1305.7404 [astro-ph.HE].

[94] O. Kalashev, D. Semikoz, and I. Tkachev, *J. Exp. Theor. Phys.* **120**, 541 (2015).

[95] M. J. Chodorowski, A. A. Zdziarski, and M. Sikora, *ApJ* **400**, 181 (1992).

[96] S. Stepney and P. W. Guilbert, *MNRAS* **204**, 1269 (1983).

[97] K. Murase and J. F. Beacom, *Phys. Rev. D* **82**, 043008 (2010), arXiv:1002.3980 [astro-ph.HE].

[98] K. Murase and E. Waxman, *Phys. Rev. D* **94**, 103006 (2016), arXiv:1607.01601 [astro-ph.HE].

[99] Y. Inoue, *Astrophys. J.* **733**, 66 (2011), arXiv:1103.3946 [astro-ph.HE].

[100] M. Ajello *et al.*, *Astrophys. J.* **800**, L27 (2015), arXiv:1501.05301 [astro-ph.HE].

[101] K. Fang and K. Murase, *Nature Phys. Lett.* **14**, 396 (2018), arXiv:1704.00015 [astro-ph.HE].

[102] K. Murase, M. Ahlers, and B. C. Lacki, *Phys. Rev. D* **88**, 121301(R) (2013), arXiv:1306.3417 [astro-ph.HE].

[103] A. De Angelis *et al.* (e-ASTROGAM), *Exper. Astron.* **44**, 25 (2017), arXiv:1611.02232 [astro-ph.HE].

[104] A. Moiseev and O. B. O. T. A. Team, *The Fluorescence detector Array of Single-pixel Telescopes: Contributions to the 35th International Cosmic Ray Conference (ICRC 2017)*, PoS **ICRC2017**, 798 (2018).

[105] M. G. Aartsen *et al.* (IceCube), *Eur. Phys. J. C* **79**, 234 (2019), arXiv:1811.07979 [hep-ph].

[106] M. Aartsen *et al.* (IceCube-Gen2 Collaboration), (2014), arXiv:1412.5106 [astro-ph.HE].

[107] T. Aramaki, P. Hansson Adrian, G. Karagiorgi, and H. Odaka, (2019), arXiv:1901.03430 [astro-ph.HE].

[108] Y. Inoue, K. Murase, G. M. Madejski, and Y. Uchiyama, *Astrophys. J.* **776**, 33 (2013), arXiv:1308.1951 [astro-ph.CO].

[109] A. Levinson, *Phys. Rev. Lett.* **85**, 912 (2000).

[110] J. Aleksic, S. Ansoldi, L. Antonelli, P. Antoranz, A. Babic, *et al.*, *Science* **346**, 1080 (2014), arXiv:1412.4936 [astro-ph.HE].

[111] A. P. Szabo and R. J. Protheroe, *Astropart. Phys.* **2**, 375 (1994), arXiv:astro-ph/9405020 [astro-ph].

[112] F. W. Stecker and M. H. Salamon, *TeV gamma-ray astrophysics: Theory and observations. Proceedings, Workshop, Heidelberg, Germany, October 3-7, 1994*, *Space Sci. Rev.* **75**, 341 (1996), arXiv:astro-ph/9501064 [astro-ph].

[113] J. Alvarez-Muniz and P. Mészáros, *Phys. Rev. D* **70**, 123001 (2004), arXiv:astro-ph/0409034 [astro-ph].

[114] Y. Inoue and A. Doi, *Publ. Astron. Soc. Jap.* **66**, L8 (2014), arXiv:1411.2334 [astro-ph.HE].

[115] Y. Inoue and A. Doi, *Astrophys. J.* **869**, 114 (2018), arXiv:1810.10732 [astro-ph.HE].

## 1. Time Scales for Thermal Particles

To accelerate particles through stochastic acceleration in turbulence, the Coulomb relaxation time scales of particles at their injection energy should be longer than the dissipation time scale. Also, in order to form the two-temperature corona that is often discussed in the literature (e.g., [66, 67]), the dissipation time scale should be shorter than the proton-electron relaxation time. We discuss these plasma time scales in this subsection. The infall time scale is expected to be similar to that of the advection dominated accretion flow [47, 48]:

$$t_{\text{fall}} \approx \frac{R}{\alpha V_K}, \quad (\text{S1})$$

where  $\alpha$  is the viscous parameter in the accretion flow [61]. Assuming that the dissipation in the corona is related to some magnetic process like reconnections, the dissipation time scale can be expressed as

$$t_{\text{diss}} \approx \frac{H}{V_A} \approx \frac{R}{V_K} \sqrt{\frac{\beta}{2}}. \quad (\text{S2})$$

The relaxation times for electrons and protons are estimated to be [49, 52]

$$t_{ee,\text{rlx}} \approx \frac{4\sqrt{\pi}\theta_e^{3/2}}{n_p\sigma_T c \ln \Lambda}, \quad (\text{S3})$$

$$t_{pp,\text{rlx}} \approx \frac{4\sqrt{\pi}\theta_p^{3/2}}{n_p\sigma_T c \ln \Lambda} \left( \frac{m_p}{m_e} \right)^2, \quad (\text{S4})$$

$$t_{pe,\text{rlx}} \approx \sqrt{\frac{\pi}{2}} \frac{(\theta_p + \theta_e)^{3/2}}{n_p\sigma_T c \ln \Lambda} \left( \frac{m_p}{m_e} \right), \quad (\text{S5})$$

where  $\theta_i = k_B T_i / (m_i c^2)$  ( $i = p$  or  $e$ ),  $\ln \Lambda \sim 20$  is the Coulomb logarithm, and we may consider a proton-electron plasma [29]. We plot these time scales as a function of  $L_X$  in Fig. S1 for  $\beta = 1$  and  $\alpha = 0.1$ . We see that among the five time scales  $t_{ee,\text{rlx}}$  and  $t_{pp,\text{rlx}}$  are the shortest and longest, respectively. This means that electrons are easily thermalized while nonthermal protons are naturally expected and could be accelerated through stochastic acceleration. Also, because  $t_{\text{diss}} \lesssim t_{pe,\text{rlx}}$  is satisfied for the range of our interest, one may expect the two-temperature corona to be formed.

## 2. Time Scales for High-Energy Protons

Nonthermal proton spectra are determined by the balance among the acceleration, cooling, and escape processes. We consider stochastic acceleration by turbulence, and take account of infall and diffusion as escape processes. We also treat inelastic  $pp$  collisions, photomeson production, Bethe-Heitler pair production, and synchrotron radiation as cooling processes.

The stochastic acceleration is modeled as a diffusion phenomenon in momentum or energy space (e.g., [53, 55, 56]). Assuming gyro-resonant scattering through the turbulence with a power spectrum of  $P_k \propto k^{-q}$ , the acceleration time is written as [73, 76, 80, 81, 84]

$$t_{\text{acc}} \approx \eta \left( \frac{V_A}{c} \right)^{-2} \frac{R}{c} (eBR)^{q-2} \varepsilon_p^{2-q}, \quad (\text{S6})$$

where  $\eta^{-1} = 8\pi \int P_k dk / B_0^2$  is the turbulence strength parameter and  $V_A = B / \sqrt{4\pi m_p n_p}$  is the Alfvén velocity. The infall time is given by Eq. (S1). Using the same scattering process for the stochastic acceleration, the diffusive escape time is estimated to be [73, 76, 80]

$$t_{\text{diff}} \approx \frac{9R}{c\eta} (eBR)^{2-q} \varepsilon_p^{q-2}. \quad (\text{S7})$$

The cooling rate by  $pp$  inelastic collisions is estimated to be

$$t_{pp}^{-1} \approx n_p \kappa_{pp} \sigma_{pp} c, \quad (\text{S8})$$

where  $\sigma_{pp}$  and  $\kappa_{pp} \approx 0.5$  are the cross section and inelasticity for  $pp$  interactions, as implemented in Refs. [82, 83]. The photomeson production energy loss rate is calculated by

$$t_{p\gamma}^{-1} \approx \frac{c}{2\gamma_p^2} \int_{\bar{\varepsilon}_{\text{th}}}^{\infty} d\bar{\varepsilon}_\gamma \sigma_{p\gamma} \kappa_{p\gamma} \bar{\varepsilon}_\gamma \int_{\bar{\varepsilon}_\gamma/(2\gamma_p)}^{\infty} d\varepsilon_\gamma \varepsilon_\gamma^{-2} \frac{dn_\gamma}{d\varepsilon_\gamma}, \quad (\text{S9})$$

where  $\gamma_p = \varepsilon_p / (m_p c^2)$  is the proton Lorentz factor,  $\bar{\varepsilon}_{\text{th}} \approx 145$  MeV is the threshold energy for the photomeson production,  $\bar{\varepsilon}_\gamma$  is the photon energy in the proton rest frame,  $\sigma_{p\gamma}$  and  $\kappa_{p\gamma}$  are the cross section and inelasticity, respectively, and the normalization is given by  $\int d\varepsilon_\gamma \varepsilon_\gamma (dn_\gamma / d\varepsilon_\gamma) \approx (1 + \tau_T) L_{\text{bol}} / (2\pi R^2 c)$ . We utilize the fitting formula based on GEANT4 for  $\sigma_{p\gamma}$  and  $\kappa_{p\gamma}$ , which are used in Ref. [92]. The Bethe-Heitler cooling rate is written in the same form of Eq. (S9) by replacing the cross section and inelasticity with  $\sigma_{\text{BH}}$  and  $\kappa_{\text{BH}}$ , respectively, where we use the fitting formula given in Refs. [95] and [96]. Finally, the synchrotron time scale for protons is given by

$$t_{p,\text{syn}} \approx \frac{6\pi m_p^4 c^3}{m_e^2 \sigma_T B^2 \varepsilon_p}. \quad (\text{S10})$$

We plot the times scales in Fig. S2 with a parameter set of  $r = 30$ ,  $\beta = 1$ ,  $\alpha = 0.1$ ,  $\eta = 10$ , and  $q = 5/3$ . We can see that particle acceleration is limited by interactions with photons except for  $L_X = 10^{42}$  erg s $^{-1}$ . For the lowest-luminosity case, the photomeson production, the Bethe-Heitler process, the  $pp$  reaction, and the diffusive escape rates are comparable to the acceleration rate around  $10^6$  GeV, while the Bethe-Heitler process hinders the acceleration for the other cases at  $\sim 10^5 - 10^6$  GeV due to a softer spectrum for a higher-luminosity Seyfert galaxy that has a lower maximum energy due to its larger photon number density.

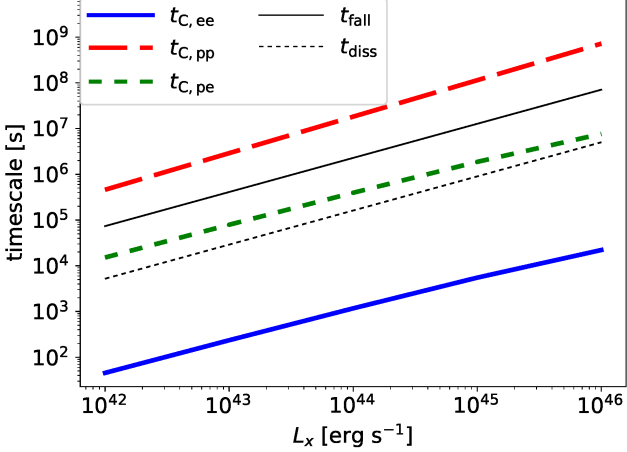


FIG. S1. The infall time and Coulomb relaxation time scales as a function of  $L_X$ .

### 3. Spectra of Nonthermal Protons

To obtain the spectrum of nonthermal protons, we solve the Fokker-Planck equation given in Eq. (1) using the Chang-Cooper method [77, 78]. The resulting spectra are shown in Fig. 2. We tabulate the critical energy for protons,  $\varepsilon_{p,\text{cl}}$ , at which the acceleration balances with loss processes in Table S1. For a lower value of  $L_X$ , the critical energy is higher owing to their lower loss rates. We consider two cases, which give similar proton spectra.

The dissipation rate in the coronae is expected to be proportional to  $L_X$ , so we may write the injection function as,

$$\dot{f}_{p,\text{inj}} = \frac{f_{\text{inj}} L_X}{4\pi \varepsilon_{\text{inj}}^3 \pi R^3} \delta(\varepsilon_p - \varepsilon_{\text{inj}}), \quad (\text{S11})$$

where  $\varepsilon_{\text{inj}}$  is the injection energy and  $f_{\text{inj}}$  is the injection fraction. The values of  $\varepsilon_{\text{inj}}$  and  $f_{\text{inj}}$  do not affect the resulting spectral shape as long as  $\varepsilon_{\text{inj}} \ll \varepsilon_{p,\text{cl}}$ . For example, if we use  $\varepsilon_{\text{inj}} = 1.5m_p c^2$ , the resulting spectrum is shown in Fig. 2 corresponds to  $f_{\text{inj}} = 5 \times 10^{-8}$ . Note that  $f_{\text{inj}}$  is larger as  $\varepsilon_{\text{inj}}$  is higher. For  $\varepsilon_{\text{inj}} < \varepsilon_p \ll \varepsilon_{p,\text{cl}}$ , the stochastic acceleration mechanism predicts a very hard spectrum,  $dN_{\text{CR}}/d\varepsilon_p \propto \varepsilon_p^{1-q}$ .

For  $L_X \gtrsim 10^{43} \text{ erg s}^{-1}$ , owing to the inefficient escape processes, the accelerated particles pile up around  $\varepsilon_p \sim \varepsilon_{p,\text{cut}}$ , which creates a hardening feature around  $\varepsilon_p \sim 0.1\varepsilon_{p,\text{cl}}$  and a strong cutoff above  $\varepsilon_p \sim 2\varepsilon_{p,\text{cl}}$ . Note that in our model the energy density of these nonthermal protons are much lower than that of the thermal protons:  $P_{\text{CR}}/P_{\text{th}}$  is of the order of  $10^{-2}$  for all the cases, where  $P_{\text{CR}} = \int d\varepsilon_p (dn_{\text{CR}}/d\varepsilon_p) \varepsilon_p / 3$  and  $P_{\text{th}} \approx n_p k_B T_p$ . Hence, these nonthermal protons do not affect the dynamical structure [52].

TABLE S1. Physical quantities related to nonthermal particles for a given  $L_X$ .

w.o. secondary reacceleration					
$\log L_X \text{ [erg s}^{-1}]$	$\log t_{\text{fall}} \text{ [s]}$	$\varepsilon_{p,\text{cl}} \text{ [TeV]}$	$\varepsilon_{e,\text{cl}} \text{ [MeV]}$	$B \text{ [kG]}$	
42.0	4.87	200	< 1	3.4	
43.0	5.61	150	< 1	1.3	
44.0	6.36	120	< 1	0.53	
45.0	7.11	84	< 1	0.21	
46.0	7.85	60	< 1	0.085	
w. secondary reacceleration					
$\log L_X \text{ [erg s}^{-1}]$	$\log t_{\text{fall}} \text{ [s]}$	$\varepsilon_{p,\text{cl}} \text{ [TeV]}$	$\varepsilon_{e,\text{cl}} \text{ [MeV]}$	$B \text{ [kG]}$	
42.0	4.87	370	22	1.9	
43.0	5.61	260	21	0.77	
44.0	6.36	200	16	0.31	
45.0	7.11	140	11	0.12	
46.0	7.85	100	6	0.049	

### 4. Time Scales for High-Energy Pairs

Even if primary electrons are not accelerated through the turbulence due to their efficient Coulomb losses, electron-positron pairs injected via hadronic processes and populated via electromagnetic cascades processes can be accelerated to higher energies without suffering from Coulomb losses [84]. Such high-energy pairs may rapidly cool down by synchrotron and inverse Compton emissions. In Seyferts, the energy of the dominant target photons for inverse Compton scatterings is around  $1 - 10 \text{ eV}$ , implying that the Klein-Nishina effect is unimportant at  $\varepsilon_e \lesssim 100 - 300 \text{ GeV}$ . If the secondary pairs can be accelerated by the turbulence, the acceleration and cooling is expected to balance at the critical energy,  $\varepsilon_{e,\text{cl}}$ , and this effect is relevant if  $\varepsilon_{e,\text{cl}}$  is higher than the energy of the thermal protons. The time scale of the reacceleration by the turbulence is given by Eq. (S6) above the thermal energy of protons,  $k_B T_p \sim 5r_{1.5} \text{ MeV}$ . Below this energy, the turbulent power spectrum should become steeper due to kinetic effects [85], and the reacceleration time is considerably longer than that by Eq. (S6).

The synchrotron cooling time scale is

$$t_{e,\text{sync}} \approx \frac{6\pi m_e c}{\sigma_T B^2 \gamma_e}, \quad (\text{S12})$$

where  $\gamma_e = \varepsilon_e/(m_e c^2)$  is the electron Lorentz factor. Then, the inverse Compton cooling time in the Thomson limit is estimated to be

$$t_{\text{IC}} \approx \frac{3m_e c}{4\sigma_T U_\gamma \gamma_e}, \quad (\text{S13})$$

where  $U_\gamma$  is the target photon energy density. Note that the Klein-Nishina effect is taken into account in the calculations of photon spectra presented in the main text.

We plot the time scales for high-energy pairs in Fig. S3, where thin and thick lines are for the cases with and without reacceleration, respectively. For the case without reacceleration,  $\varepsilon_{e,\text{cl}} < 1 \text{ MeV}$ . When this energy is

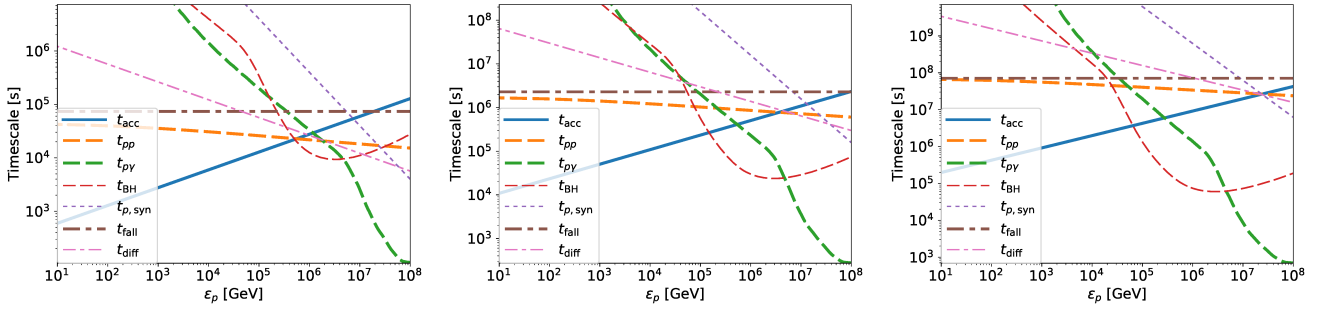


FIG. S2. Comparison of time scales for high-energy protons in the cases with  $L_X = 10^{42}$  erg s $^{-1}$  (top),  $10^{44}$  erg s $^{-1}$  (middle), and  $10^{46}$  erg s $^{-1}$  (bottom).

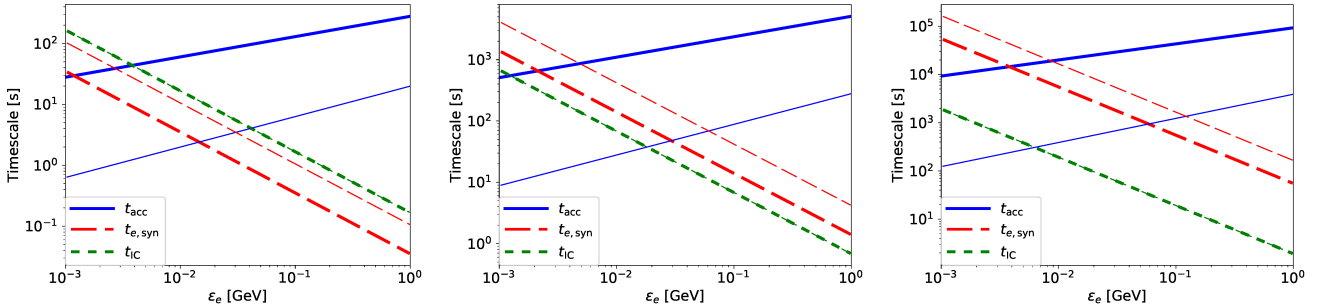


FIG. S3. Comparison of time scales for high-energy electrons and positrons in the cases with  $L_X = 10^{42}$  erg s $^{-1}$  (left),  $10^{44}$  erg s $^{-1}$  (middle), and  $10^{46}$  erg s $^{-1}$  (right).

lower than the thermal energy of protons, the waves are expected to be dissipated, and the stochastic acceleration of electrons is unlikely in all the range of  $L_X$ . For the case with reacceleration, the electrons can be maintained with energies between 6 – 22 MeV, depending on  $L_X$  (see Table S1). For  $L_X = 10^{42}$  erg s $^{-1}$ , the synchrotron cooling is more likely to be important, while

for  $L_X \gtrsim 10^{43}$  erg s $^{-1}$ , the inverse Compton cooling is dominant. The critical electron energy,  $\varepsilon_{e,cl}$ , at which the cooling and reacceleration balance with each other is lower for a higher value of  $L_X$  due to the efficient inverse Compton cooling. When the critical energy is higher than the thermal proton temperature, the reacceleration can occur.